Estimating Loadability Region of Natural Gas System via Monotone Inner Polytope Sequence

Dan Wu,[†] Member, IEEE, Tiantian Nie,^{*} Konstantin Turitsyn,[†] Member, IEEE, and Seth Blumsack,[‡] Member, IEEE

Abstract-Natural gas network is important for residential heating, industrial manufacturing, and electricity generation. Although it is reliable and resilient to local disruptions, extreme situations such as natural disasters and political conflicts can degenerate its capability of gas transportation and delivery, influencing other social activities. Evaluating loadability regions of natural gas networks is hard due to nonlinear constraints. This paper proposes a fast computational tool for feasibility screening of natural gas load profiles. It first establishes the theoretical results on the convexity of loadability regions with sufficient conditions. Then, an asymptotic algorithm is applied to compute a sequence of inner polytopes that converges to the convex loadability region. Each polytope in the sequence can serve as a certificate for feasibility. The conservativeness of this inner estimation will decline along the monotone sequence. The algorithm is testified on a modified realistic Belgian natural gas system with multi-dimensional load profiles.

Index Terms—Natural gas system, loadability region, convexity, inner polytope sequence

I. INTRODUCTION

Natural gas is one of the primary energy sources for the modern society in residential heating, industrial manufacturing, and electricity generation. The abundance, availability, affordability, and low-carbon emission make it competitive to most of other energy sources [1], [2]. According to the U.S. Energy Information Administration (EIA), the U.S. marketed natural gas production kept increasing since 2005 from 51.85 billion cubic feet per day (Bcf/day) to 78.94 Bcf/day in 2017, and is expected to increase further in 2019. The major increase of the consumption is attributed to electric power sector [3]. The EIA expects that the total utility-scale electricity generation from natural gas will rise from 32% in 2017 to 35% in 2019.

As the gas network and the power network becoming closely interconnected, there arises opportunities to co-optimize both systems simultaneously. Some research works [4]–[7] proposed integrated optimization frameworks that include both the optimal power flow and the optimal gas flow. To accurately mimic the gas flow transient behaviors, [8]–[11] included the dynamical models for the gas flow. Other works attempted to analyze disturbances or risks for the interconnected system, for example, [8] discussed possibilities of using gas-fired power

†: Massachusetts Institute of Technology, Department of Mechanical Engineering, danwumit@mit.edu, turitsyn@mit.edu, *: University of North Carolina at Charlotte, Department of Systems Engineering and Engineering Management, tnie1@uncc.edu, ‡: Pennsylvania State University, College of Earth and Mineral Sciences, and Santa Fe Institute, sethb@psu.edu

plant to compensate wind power fluctuations; [12] considered financial risks for the electric companies.

Although interactions are bidirectional between power and natural gas systems, the dependence of power on gas prevails. For example, the development of shale gas technology enables the natural gas sector in electricity generation to increase in recent years, occupying over one third of the total electricity generation [3]. It exposes a potential risk that a breakdown of gas network can substantially influence the interconnected power grid. On the other hand, the natural gas systems are primarily designed to be self-sustainable by the gas itself. Technical report [13] examined how the power grids' failures can influence gas systems. It concluded that natural gas networks are very reliable and resilient to the local short-term disruptions of electricity. Only large scale long term electricity outage can cause serious failures in gas networks [13]. This biased dependence between power and gas systems indicates that a reliable and resilient gas network design can serve as a good support for the high-quality operations of both systems.

While reliable and resilient from local electricity failures, extreme situations such as earthquakes, hurricanes, and terrorist attacks may affect the functionality of the gas system and degenerate its delivery capability. For example, in 2005 Hurricanes Katrina and Rita disrupted the U.S. oil and gas production [14]; in 2013 terrorist's attacks on the Amenas gas plant reduced 10% of Algerian gas production. To address these situations, [15]–[17] proposed performance indices to evaluate disastrous resilience of natural gas networks. [18] evaluated seismic vulnerability of interdependent gas and electricity systems.

In the extreme case when a gas network is damaged, a thorough evaluation should be conducted to understand the system's degenerated loadability. This information is beneficial for gas utilities to schedule future delivery plans. It can also serve as the critical information for other interconnected systems. A traditional co-optimization model for both systems can achieve this goal [4]-[7]. However, combining two large complex systems together makes the problem much more challenging to solve. Each system may not be able to share the actual model in the co-optimization because of conflicts of interests, security and confidentiality concerns. Therefore, pre-evaluations of the gas loadability region with simple descriptions are more practical for exchanging least amount of information among interconnected systems. Such evaluation needs to be computationally achievable and properly accurate to ensure reliable functionality for the normal and post-disaster operations. If multiple uncertain loads exists,

2

In this paper we first show the convexity of injection region for the steady state gas flow model under certain conditions, which further yields the convex loadability region of the gas network. Then, we apply a sequential optimization algorithm to approximate this convex loadability region by a sequence of polytopes. Each polytope in the sequence can serve as an inner estimation of the loadability region, and guarantees feasibility of any load profile inside the polytope. The proposed method is particularly favorable for fast feasibility screenings of load profiles in large quantities, and a compromise of conservativeness can be controlled. The major contributions of the paper are listed below.

- It shows that the injection region of natural gas is convex under certain conditions, which further indicates the convexity of gas loadability region.
- It proposes a monotone inner polytope sequence to approximate the convex loadability region with asymptotic convergence and conservativeness control.
- 3) It applies a sequential optimization algorithm to compute the proposed monotone inner polytope sequence.

The rest of the paper is organized as follow. Section II describes the gas network model that is used in the paper. Section III modified the model for simplicity. The main theoretical results are presented in Section IV. Section V describes the monotone inner polytope sequence and the algorithm to construct it. Numerical simulations are provide in Section VI. Setion VII concludes the paper.

II. NATURAL GAS SYSTEM MODEL

This section describes the steady state natural gas network model. Consider a natural gas network as a graph $\mathcal{G}(\mathcal{V},\mathcal{E})$ with the node set $\mathcal{V} := \{1, 2, \cdots, n\}$ and the branch set $\mathcal{E} := \{1, 2, \cdots, m\}$. We say node-i and node-j are adjacent nodes if there is one pipeline segment connecting them. Nodek is said to be an upstream node of node-i if there exists a directed path connecting them by following the flow direction from k to i. Similarly, node-j is a downstream node of node-iif there is a directed path connecting them by following the flow direction from i to j. A source node is a node without upstream nodes. A sink node (load node) is a node without downstream nodes. Node-i is called a merging node if it has multiple adjacent upstream nodes. Node-j is called a splitting *node* if it has multiple adjacent downstream nodes. Node-k is called a transitive node if it only has one adjacent upstream node and one adjacent downstream node. A node with both multiple adjacent upstream nodes and adjacent downstream nodes can always be represented by one merging node and one splitting node.

The natural gas network is also subjected to the physical laws of natural gas such as pressure-flow Weymouth equations and mass conservation law, as well as engineering requirements such as compressors and pressure limits.

A. Weymouth Model

The steady state gas flow describes the relation between pipeline mass flow rate and the corresponding node pressures. Ignoring transient dynamics, a classical compressible steady state gas flow model which is commonly used in natural gas pipelines is called the "Weymouth model"

$$\lambda_{i,j}(\pi_i^2 - \pi_j^2) = \psi_{i,j}|\psi_{i,j}| \tag{1}$$

where π_i is the gas pressure at node-i, $\psi_{i,j}$ is the gas flow rate through pipeline-(i,j), $\lambda_{i,j}>0$ is a pre-calculated constant which is related to pipeline parameters, gas properties, etc.

Let $P \in \mathbb{R}^n$ be the column vector of $[\pi_i^2]$, $\mathbf{C} \in \mathbb{R}^{m \times n}$ be the incidence matrix of $\mathcal{G}(\mathcal{V}, \mathcal{E}), \psi \in \mathbb{R}^m$ be the column vector of flow $[\psi_{i,j}]$, and $\mathbf{M}(\lambda) \in \mathbb{R}^{m \times m}$ be the diagonal matrix of $[\frac{1}{\lambda_{i,j}}]$. If we choose the graph direction to be the flow direction and assume it is fixed¹, then the absolute operator in (1) can be removed, yielding

$$\mathbf{C}P = \mathbf{M}(\lambda)\psi^2 \tag{2}$$

where ψ^2 represents the pointwise square, and $\psi \geq 0$.

B. Mass Flow Conservation Law

The gas system must preserve the total mass flow rate at every node. It states that the total gas flow entering a node should equal to the total gas flow leaving the node. Therefore, we have

$$\sum_{i:i\to k} \psi_{i,k} + \phi_{k,in} = \sum_{j:k\to j} \psi_{k,j} + \phi_{k,out}$$
 (3)

for every $k \in \mathcal{V}$.

Let $\phi \in \mathbb{R}^n$ be the column vector of $[\phi_{k,in} - \phi_{k,out}]$, then (3) can be written as

$$\mathbf{C}^T \psi = \phi \tag{4}$$

C. Compressors

Compressors are active components in the gas system which boost up gas pressures to achieve engineering requirements in the network.

The boosting process inevitably consumes energy. Some compressors are driven by electric power, thus are modeled as power load. Some are driven by gas combustion, hence are modeled as gas load. The mathematical description of a gas load compressor is

$$P_i = K_{i,j} P_i \tag{5a}$$

$$H_{i,j} = \beta_{i,j} (K_{i,j}^{\theta_{i,j}} - 1) \psi_{i,j}$$
 (5b)

$$\Delta \phi_{i,j} = a_{i,j} + b_{i,j} H_{i,j} + c_{i,j} H_{i,j}^2$$
 (5c)

where $K_{i,j}$ is the boosting ratio; $\beta_{i,j}$, $\theta_{i,j}$, $a_{i,j}$, $b_{i,j}$, and $c_{i,j}$ are pre-determined parameters; $\Delta \phi_{i,j}$ is the consumed gas flow. One can further substitute (5b) into (5c) and get

$$\Delta \phi_{i,j} = \hat{a}_{i,j} + \hat{b}_{i,j} \psi_{i,j} + \hat{c}_{i,j} \psi_{i,j}^2$$
 (6)

¹This assumption will be further discussed in Section IV

D. Engineering Requirements

There are several engineering and operational requirements for gas networks. In this paper we consider the node pressure limits

$$P_{min} \le P \le P_{max} \tag{7}$$

and the compressor ratio limits

$$1 \le K_{i,j} \le K_{i,j,max} \tag{8}$$

III. NETWORKS WITH IDEAL COMPRESSORS

Section II has discussed a static natural gas network model. To establish the convexity result in a simple way, we will idealize the compressor model in this section with a mild assumption, and discuss how to remove ideal compressors while preserving equivalence.

A. Ideal Compressors

In Subsection II-C we provided a detailed compressor model which is driven by gas combustion. Assume that the amount of gas consumed by the compressor is much smaller than the bulk gas flow through the compressor, then simplify (5) as

$$P_j = K_{i,j} P_i (9a)$$

$$1 \le K_{i,j} \le K_{i,j,max} \tag{9b}$$

where i is a fictitious node at which the compressor takes in gas flow, j is another fictitious node at which the compressor outputs gas flow. These nodes are defined arbitrarily close to the compressor in the middle of a pipeline (see Figure 1(a)).

Denote the set of these fictitious nodes as V_f , and the set of compressors as \mathcal{E}_c , then our refined network graph is given by $\mathcal{G}_c := \mathcal{G}(\mathcal{V} \cup \mathcal{V}_f, \mathcal{E} \cup \mathcal{E}_c)$.

B. Network Splitting

Note that the pressures on two fictitious nodes of a compressor are not determined by the Weymouth model in (2) with respect to the flow, but determined by the linear scaling relation in (9a); while the mass flow conservation law (4) still preserves. One can split the entire network \mathcal{G}_c into $|\mathcal{E}_c|+1$ many individual sub-networks $\{\mathcal{G}_s, s=1,2,\cdots,|\mathcal{E}_c|+1\}$ by removing every compressor from the network. The split network and the original network are equivalent as long as every pair of fictitious nodes associated with the same compressor satisfies pressure relation in (9a) and mass conservation law.

Without loss of generality, consider a network \mathcal{G}_c with only one compressor (see Figure 1(a)). It can be separated into two individual sub-networks by removing the compressor as shown in Figure 1(b). Let's label the sub-network on the left of Figure 1(b) as \mathcal{G}_1 , and the one on the right of Figure 1(b) as \mathcal{G}_2 . Then, the union of two sub-networks \mathcal{G}_1 and \mathcal{G}_2 is equivalent to the original network \mathcal{G}_c if and only if

$$P_j = K_{i,j} P_i \tag{10a}$$

$$\phi_i = \phi_i \tag{10b}$$

where i and j are the fictitious nodes associated with the compressor.

The network splitting technique will be revisited through the proof of convexity in Appendix A. (a) Before Splitting

(b) After Splitting

Fig. 1: Ideal Compressor and Network Splitting

IV. CONVEXITY OF GAS INJECTION REGION

According to the models from Section II and III, this section establishes the convexity results of this paper. The proof for the main theorem is provided in Appendix A.

A. Injection Region of Natural Gas System

(2), (4), (7), and (9) provide a standard description of natural gas network. We list them together as

$$\mathbf{C}P = \mathbf{M}(\lambda)\psi^2 \tag{11a}$$

$$\mathbf{C}^T \psi = \phi \tag{11b}$$

$$P_i = K_{i,j} P_i \tag{11c}$$

$$P_{min} \le P_j \le P_{max} \tag{11d}$$

$$1 \le K_{i,j} \le K_{i,j,max} \tag{11e}$$

$$\psi > 0 \tag{11f}$$

Note that (11) is an under-determined system, given a load profile ϕ . Thus, gas network operators can take this flexibility to optimize some cost and reach a unique operating point. However, not every choice of ϕ admits a feasible solution to (11). Therefore, we define the *injection region* $\mathscr J$ of a natural gas network as

$$\mathscr{J} := \{ \phi \in \mathbb{R}^n \mid (11) \text{ is nonempty} \}$$
 (12)

where ϕ includes every node injection in the network.

Furthermore, we define the *loadability region* \mathcal{L} of a natural gas network as the projection of \mathcal{J} for sink nodes

$$\mathcal{L} := \{ \phi \text{ on } sink \text{ node } | \text{ (11) is } nonempty \}$$
 (13)

B. Convexity of Gas Injection Region

We list three conditions which together suffice the convexity of gas injection region, yielding the convexity of the corresponding loadability region. Failure of these conditions can result in non-convexity of gas injection region. However, it does not necessarily result in non-convexity of the gas loadability region. One of our future work is to relax these conditions for preserving convexity of the gas loadability region.

2) Flow direction is fixed for every branch.

4

3) All the node pressure ranges are identical.

Condition 1 guarantees the solution of node pressure P given a branch flow ψ , and helps construct a feasible pressure profile for the proof. Condition 2 is a mild assumption since the reverse of flow direction seldom happens or happens very slowly in practice. Condition 3 provides a suitable range for ensuring the required feasible pressure profile in the proof. These conditions will be revisited in the proof in Appendix I.

The basic idea of convexity is to show that any point on the line segment between two feasible gas injection profiles is feasible. We start with two arbitrary feasible injection profiles, ϕ_a and $\phi_b \in \mathscr{J}$, where subscript a and b differentiate two injection profiles. Let ψ_a and P_a be the branch flow and node pressure associated with ϕ_a ; ψ_b and P_b be the branch flow and node pressure associated with ϕ_b . Define

$$\phi_c := (1 - \mu)\phi_a + \mu\phi_b \tag{14}$$

where $\mu \in [0, 1]$. Then, we have two lemmas as follow.

Lemma 1. $\psi_c := (1 - \mu)\psi_a + \mu\psi_b$ is the only branch flow corresponds to load profile ϕ_c .

Proof of Lemma 1: Consider

$$\mathbf{C}^T \psi_c = \mathbf{C}^T ((1 - \mu)\psi_a + \mu \psi_b)$$
 (15a)

$$= (1 - \mu)\mathbf{C}^T \psi_a + \mu \mathbf{C}^T \psi_b \tag{15b}$$

$$= (1-\mu)\psi_a + \mu\psi_b \tag{15c}$$

$$= \phi_c \tag{15d}$$

Hence ψ_c is a branch flow solution with respect to ϕ_c .

On the other hand, suppose there exists another branch flow ψ_d which corresponds to ϕ_c , then $\mathbf{C}^T(\psi_c - \psi_d) = 0$. By Condition 1, \mathbf{C}^T has full column rank. Thus, $\psi_c - \psi_d = 0$ which yields the uniqueness.

Lemma 2. The branch flow ψ_c admits at least one node pressure profile P_c .

Proof of Lemma 2: By Condition 1, C has full row rank. So $\mathbf{C}P = \mathbf{M}(\lambda)\psi^2$ has at least one solution for any given ψ . Thus, $\psi = \psi_c$ results in at least one solution P_c .

Lemma 1 and 2 indicate that any injection profile ϕ_c on the line segment between ϕ_a and ϕ_b has and only has one branch flow ψ_c which further admits node pressure profile P_c .

Theorem 1. Consider a natural gas network \mathcal{G}_c with an ideal compressor described by (9), under Conditions 1, 2 and 3, its injection region \mathcal{J} is a convex set.

The proof of Theorem 1 is long and omitted here. Details are provided in Appendix A.

Corollary 1. Consider a natural gas network \mathcal{G}_c with $h \in \mathbb{Z}_+$ many ideal compressors described by (9), under Conditions 1, 2 and 3, its injection region \mathcal{J} is a convex set.

The proof of this corollary follows the same arguments as in the proof of Theorem 1.

Corollary 2. Consider a natural gas network \mathcal{G}_c with $h \in \mathbb{Z}_+$ many ideal compressors described by (9), under Conditions 1, 2 and 3, its loadability region \mathcal{L} is a convex set.

The proof of this corollary follows the argument that the projection of a convex set is also convex.

V. ESTIMATING CONVEX LOADABILITY REGION

The above section reveals that a natural gas system can have a convex loadability region under sufficient conditions. The convexity property favors the estimation of the loadability region via a simple algorithm in this section. Specifically, it focuses on how to use a particular type of polytope sequence to approximate a convex set. A detailed algorithm is provided for computing this sequence at any given length.

A. Monotone Inner Polytope Sequence

Generically, understanding a semi-algebraic set is hard in the sense of computational complexity. However, if the set is convex, it can be approximated by the limit of a sequence of polytopes. Each polytope in the sequence is regarded as an estimation of the set. To guarantee feasibility, we require every element in the sequence is inscribed in the convex set.

Mathematically, consider a convex set \mathcal{P} . We say a sequence $\{\mathcal{P}_k\}_{k=1,2,\cdots}$ of polytopes \mathcal{P}_k to be the *inner polytope sequence of* \mathcal{P} if

- 1) For any $\mathcal{P}_i \in \{\mathcal{P}_k\}, \ \mathcal{P}_i \subseteq \mathcal{P}$
- 2) $\lim_{i\to\infty} \mathcal{P}_i = \mathcal{P}$

Furthermore, if for any i > j we have $\mathcal{P}_j \subseteq \mathcal{P}_i$, then the sequence $\{\mathcal{P}_k\}$ is said to be *monotone*.

Note that every polytope in the sequence can serve as an *estimation* of the loadability region and certify the feasibility of its enclosed points. The major advantage comes from the cheap evaluation of a set of linear inequalities. Without these polytopes, verifying feasibility requires iterative algorithms, which in general is much more expensive. If the loadability region is not convex, one can still use inner polytopes to approximate it. One approach applies the Brouwer fixed point theorem to certify the enclosed polytope is solvable [20]. However, the performance of error and convergence will not be provided.

B. Constructing Monotone Inner Polytope Sequence

This part presents a sequential optimization algorithm to construct a monotone inner polytope sequence for estimating the natural gas loadability region. The proposed algorithm is among a class of iterative approach for approximating convex bodies [21]. The pseudo-code of this algorithm is provided in Algorithm 1.

The basic iterative procedure is that at the i-th inner polytope \mathcal{P}_i identifying the furthest parallel support function for each facet \mathcal{F}_p of \mathcal{P}_i . The feasible points on the support functions are our new vertices. Using new vertices to enlarge the previous polytope to get polytope \mathcal{P}_{i+1} , and repeat this process to capture more feasible space at each iteration. The optimization routine used in Algorithm 1 is the standard

primal-dual interior point (PDIP) method². A 2-dimensional demonstration of this procedure is displayed in Figure 2.

Algorithm 1 Constructing Monotone Inner Polytope Sequence

```
1: Input system S(x;d).
                                                     \triangleright x \in \mathbb{R}^{N_x}: state variables;
     d \in \mathbb{R}^{N_d}: load variables
 2: for i = 1, 2, \dots, N_d do \triangleright generate a starting polytope
           Set cost function f_i := e_i^T d, where e_i is the unit vector
           with entry-i being 1.
           Apply PDIP solver to maximize f_i subjected to net-
 4:
           work constraints.
           Collect solution \tilde{d}_{0,i} in V_0.
 5:
 6: end for
 7: Construct the convex hull C_0 associated with V_0.
8: Let the facet set of C_0 be F_0=\{H^0_{j_0}\mid j_0=1,\cdots,J_0\}.
8: Let the facet set of C_0 be F_0 = \{H_{j_0} \mid j_0 = 1, \cdots, s_{0j}\}.

9: for k = 1, 2, \cdots, K do \triangleright K: length of sequence

10: for j_{k-1} = 1, 2, \cdots, J_{k-1} do \triangleright facet index

11: Set cost function f_{j_{k-1}} := \overrightarrow{n}_{j_{k-1}}^{k-1} d, where \overrightarrow{n}_{j_{k-1}}^{k-1} is the outer normal direction of hyperplane H_{j_{k-1}}^{k-1}.
10:
11:
                 Apply PDIP solver to maximize f_{j_{k-1}} subjected to
12:
                 network constraints.
                 Collect solution \tilde{d}_{k,j_{k-1}} in \Delta V_{k-1}.
13:
           end for
14:
           Let V_k = V_{k-1} \bigcup \Delta V_{k-1}.
15:
           Construct the convex hull C_k associated with V_k.
16:
           Let the facet set of C_k be F_k = \{H_{j_k}^k \mid j_k =
17:
            1,\cdots,J_k.
18: end for
```

The plot in Figure 2(a) shows a convex set \mathcal{P} of interests. To obtain a starting polytope, one solves optimization problems to find maximal points on each axis, for instance, point A_0 and B_0 in Figure 2(b). Based on these points a 1-D facet (A_0, A_1) is determined, and the green area (O, A_0, A_1) beneath this facet in Figure 2(b) becomes our starting polytope. Next, maximizing along the normal direction (green arrow in Figure 2(c)) of facet (A_0, A_1) provides us a new point A_1 in Figure 2(c). The new point A_1 creates two new facets (A_0, A_1) and (A_1, B_0) above the old facet (A_0, B_0) with its vertices A_0 and B_0 . The area beneath facets (A_0, A_1) and (A_1, B_0) induces the second polytope (O, A_0, A_1, B_0) . Following the same strategy the third polytope $(O, A_0, A_2, A_1, B_2, B_0)$ is shown in Figure 2(d). One can keep executing this process to infinity, leading the polytope sequence to the exact convex set \mathcal{P} . To compromise both the accuracy and the computation, usually the first few steps are enough.

Constructing polytopes to optimally approximate high dimensional convex bodies is a hard problem in general [22]. However, gas network regulations and market practice keep the variable loads of interests low dimensional. These regulations only allow a small number of variable node loads [23]. So in the real applications the loadability region of interests is usually in a low dimensional space, which is particularly

(a) Original Convex Set (b) The starting Polytope

(c) The 1^{st} Polytope (d) The 2^{nd} Polytope

Fig. 2: A 2-D Example of Algorithm 1

suitable for the proposed method.

If very high dimensional uncertain deliveries need to be investigated, some refinements can reduce the computational complexity of the proposed method. For example, instead of reconstructing a new convex hull at each step, one can update the previous convex hull by adding a new vertex at a time. Another approach may randomly select some simplices defined by the known vertices (may not be the facets of the convex hull) and compute their parallel support functions to acquire new vertices. This approach cannot guarantee the optimal selection of vertices, but can be computationally much cheaper.

C. Convergence Analysis

Estimating convex bodies by polytopes is a classical problem. Many results have been established [21], [24]–[28]. A thorough survey in this topic can be found in [22].

To establish the convergence rate, a metric needs to be defined priorly. Specifically in this paper, we use the *Nikodim metric* (also known as the *symmetric difference metric*) as follow. Given two sets U and V, the Nikodim metric

$$\rho(U, V) := \mathsf{Vol}(U \cup V) - \mathsf{Vol}(U \cap V) \tag{16}$$

where $\operatorname{Vol}(\cdot)$ is the volume operator. Note that if $V \subset U$, $\rho(U,V) = \operatorname{Vol}(U) - \operatorname{Vol}(V)$, which can be used as a measure of error for an inner estimation V of U.

Since Algorithm 1 is in the class of iterative methods for inscribed polytopes [21], [24] and the gas loadability region has the twice continuously differentiable boundary, it follows the results in [27]

$$\rho(\mathcal{P}, \mathcal{P}_k(n_k)) \to K n_k^{2/(1-N_d)}, \text{ as } n_k \to \infty$$
(17)

where \mathcal{P} is the convex loadability region; $\mathcal{P}_k(n_k)$ is the k-th polytope generated by our algorithm; n_k is the number of vertices; K is a constant with respect to the dimensionality N_d and the affine area of the surface $\partial \mathcal{P}$. It suggests that as the

²All simulations displayed in the paper were coded and executed in Matlab 2017b environment with a 2.8 GHz i7 CPU and 16 GB RAM. The specific optimization solver used during simulations was the interior-point solver from Matlab "fmincon" function with user defined gradient and Hessian functions.

The asymptotic convergence rate between two polytopes is

$$r_{conv} := \frac{\rho(\mathcal{P}, \mathcal{P}_k(n_{k+1}))}{\rho(\mathcal{P}, \mathcal{P}_k(n_k))} \to \left(\frac{n_{k+1}}{n_k}\right)^{2/(1-N_d)}$$
(18)

Since the dimensionality N_d is considered to be greater than one, $2/(1-N_d)<0$. As long as $n_{k+1}/n_k>1$ is fixed, the convergence rate $r_{conv}<1$ is also fixed. Therefore, the generated polytope sequence converges geometrically to the target convex set.

VI. NUMERICAL SIMULATIONS

This section presents simulation results based on a modified realistic natural gas system, the Belgium gas network [29]. The first part describes the network settings, while the second part presents loadability regions and estimations for this system based on the proposed algorithm.

A. Modified Belgium Gas Network

6

A detailed description of the Belgium gas network can be found in [29]. The network graph has an "almost" tree structure: it includes a few segments with parallel pipelines. A special technique is applied to equivalently represent two parallel pipelines by a single pipeline.

Fig. 3: One-Line Diagram of Belgium Gas Network

Consider two parallel pipelines described by

$$\lambda_{i,j,1}(P_i - P_j) = \Psi_{i,j,1}^2 \tag{19a}$$

$$\lambda_{i,j,2}(P_i - P_j) = \Psi_{i,j,2}^2$$
 (19b)

A single equivalent pipeline is

$$\lambda_{i,j,eq}(P_i - P_j) = \Psi_{i,j,eq}^2 \tag{20}$$

By the mass flow conservation law we have

$$\Psi_{i,j,eq} = \Psi_{i,j,1} + \Psi_{i,j,2} \tag{21}$$

Substituting (21) and (19) into (20) one obtains the equivalence condition

$$\lambda_{i,j,eq} = \left(\sqrt{\lambda_{i,j,1}} + \sqrt{\lambda_{i,j,2}}\right)^2 \tag{22}$$

After converting parallel pipelines into single ones, the modified Belgium gas network has a tree structure. We further modify it slightly for satisfying sufficient conditions in Section IV. A one-line paragram of the network graph is shown in Figure 3. The green squares represent standard nodes or junctions. The blue circles are fictitious nodes associated with compressors drawn by pink lines. Parameters of this network are computed from [29] and provided in Appendix B.

B. Estimations of Loadability Regions

To illustrate the performance of the proposed monotone inner polytope sequence, we first consider a 3-dimensional loadability region by relaxing loads at node 3, 6, and 15. All the other loads are fixed at the given values in the Appendix.

After 4.56 seconds, Algorithm 1 terminates at the third polytope of the sequence since it is appropriate to capture the majority of the loadability region. The appropriateness will be defined shortly below. Results are depicted in Figure 4. Figure 4(a) shows the starting polytope in purple with the maximal point on each axis. Based on the facet defined by those maximal points, a new vertex in green is found which gives rise to a larger green first polytope in Figure 4(b). Follow the same strategy, the second polytope in red was identified in Figure 4(c) which is much larger than the first polytope. Finally, the thrid polytope in blue is identified in Figure 4(d).

We define the *relative volume* of the k-th inner polytope \mathcal{P}_k of a convex set \mathcal{P} by the *volume ratio* R_p

$$R_p := Vol(\mathcal{P}_k)/Vol(\mathcal{P}) \tag{23}$$

However, high-dimensional volume is hard to compute. Hence, we evenly discretize each load to generate a discrete sample $pool^3$ and count the numbers of interested points to approximate R_p . Specifically,

$$R_p \approx N_k/N_p$$
 (24)

where N_k is the number of points inside polytope \mathcal{P}_k , while N_p is the number of points inside \mathcal{P} . As the size of the sample pool goes to infinity, the quotient N_k/N_p goes to R_p .

Figure 7(a) shows the Relative Volume for our 3-D example. The starting polytope, labeled index-0, occupies about 47.05% of the total volume. Since the polytope sequence is monotone, the volume increases along the sequence. At the third polytope, the volume is about 98.90%. Computations on further polytopes will not enhance the volume substantially. Therefore, the algorithm compromises between conservativeness and speed.

The next demonstration is to estimate a 4-dimensional loadability region by the proposed method. Specifically, we relax loads at node 3, 7, 16, and 20 in Figure 3 and fix all other loads at given values. Since 4-D objects cannot be displayed directly, we project the simulation results on different subspaces.

Algorithm 1 terminates at the thrid inner polytope after 8.51 seconds. Figure 5 shows the projections of polytopes on a 2-D load space at node 3 and 7. The yellow dots are the discretized points which are feasible to the gas flow problem. They roughly capture the projection of the 4-D loadability region. One can see from Figure 5(a) to Figure 5(d) that the projections of the inner polytopes gradually occupy almost the entire loadability region. The 3-D projections of these polytopes, as well as the loadability region, are shown in Figure 6. Figure 6(a)-6(d) show the projections of the polytopes on the load subspace at node 3, 7, and 16; while Figure 6(e)-6(h) depict the projections of polytopes on the load

 $^{^{3}}$ In this paper, each relaxed load is evenly sampled with 21 points. So the total number of sample points is 21^{d} , where d is the dimensionality of the loadability region.

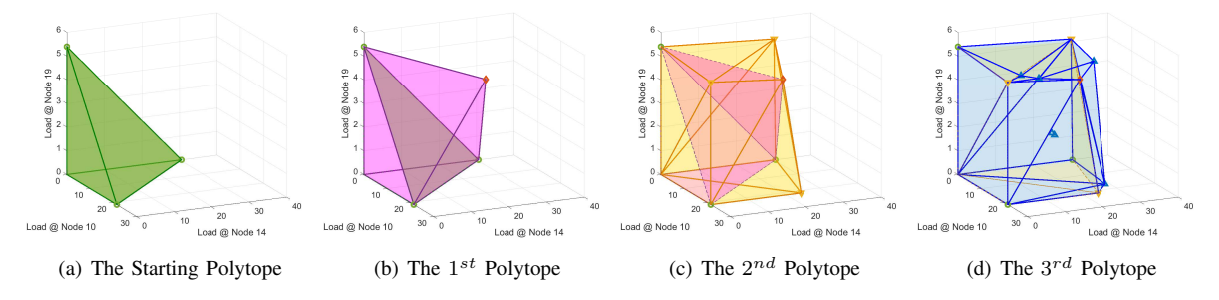


Fig. 4: Inner Estimations of 3-D Loadability Region at Node 10, 14, and 19

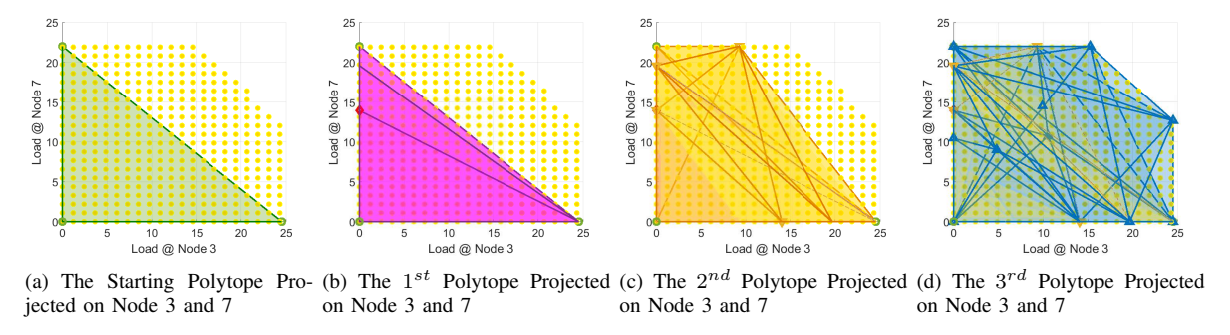


Fig. 5: 2-D Projections of Inner Estimations of 4-D Loadability Region at Node 3, 7, 16, and 20

subspace at node 3, 7, and 20. The projections of loadability region are illustrated in Figure 6(i) and 6(j) by the yellow balls. The relative volumes of these polytopes are presented in Figure 7(b). Although the starting polytope, labeled index-0 in the figure, only occupies 10.20% of the loadability region, the third polytope, labeled index-3, fills 95.19% of the total feasibility region.

C. Feasibility Screening with Inner Polytope Estimations

As discussed before, the major advantage of the inner polytope estimation is to provide a simple but accurate description of the actual loadability region. We take this advantage to screen different loading scenarios, and compare to the actual feasibility checking based on an optimization method. At a given load profile, minimizing a constant zero objective function subjected to network constraints to solve node pressures and source injections.

Consider three variable loads at node 10, 14, and 19 ranging in [0,22.5], [0,31], and [0,5.5], respectively. Each range is evenly discretized by 21 points. There are 9261 many 3-D load combinations in total to verify. Screening whether these load profiles are within the third inner polytope (shown in Figure 4(d)) takes about 0.039 seconds. However, checking the feasibility of these load profiles takes about 2575 seconds on the same computer. The gain of the computational speed is around 6.6×10^4 with a compromise of 1.1% (computed by $1-R_p$) conservativeness. A logarithmic comparison of the execution time is depicted on the left part of Figure 8.

In another scenario with four variable loads at node 3, 7, 16, and 20 with ranges of [0,25.5], [0,23], [0,19], and [0,6.5], respectively. Each load range is again evenly discretized by 21 points. Therefore, there are 194481 many 4-D

load combinations to verify. Screening if these load profiles are within the third inner polytope (shown in Figure 6(d) and 6(h)) takes about 0.095 seconds. However, checking the feasibility of these load profiles takes about 230377 seconds on the same computer. The gain of the computational speed is around 2.43×10^6 accompanied with a compromise of 4.81% conservativeness. A logarithmic comparison of the execution time is depicted on the right part of Figure 8.

These numerical results suggest that the inner polytope estimation can serve as an easy alternative of the actual loadability region for screening load profiles with limited conservativeness.

VII. CONCLUSION

This paper discusses how to make a good estimation of the loadability region of the natural gas flow problem for fast feasibility screenings. It starts with the description of classic gas flow model. Then, it defines the injection region and the loadability region, and rigorously establishes the convexity results for both regions under certain sufficient conditions. Based on the convexity property, it further applied a sequential optimization algorithm that constructs a monotone sequence of inner polytopes to approaching the loadability region. The elements in the sequence provide good estimations for the loadability region with controlled conservativeness. Finally, the paper demonstrates correctness of the theory and convergence of the algorithm on a modified realistic gas network.

The convexity result is specifically tailored for structured gas networks. One future direction is to extend the established result to other systems, for example, cyclic gas networks, or water systems. Another direction of interests would be enhancing the scalability of the proposed method by designing new update schemes for constructing convex hulls.

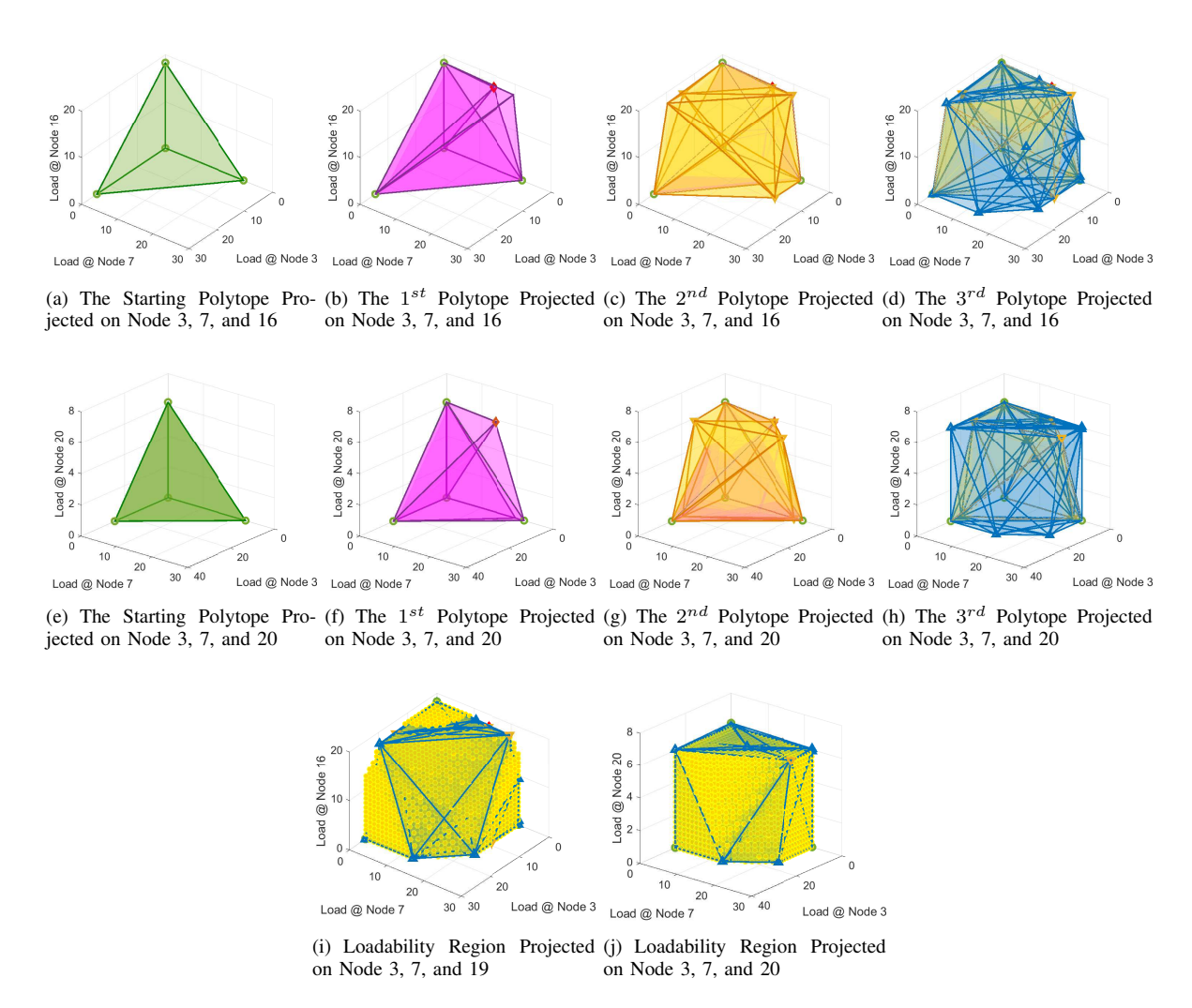


Fig. 6: 3-D Projections of Inner Estimations and Loadability Region at Node 3, 7, 16, and 20

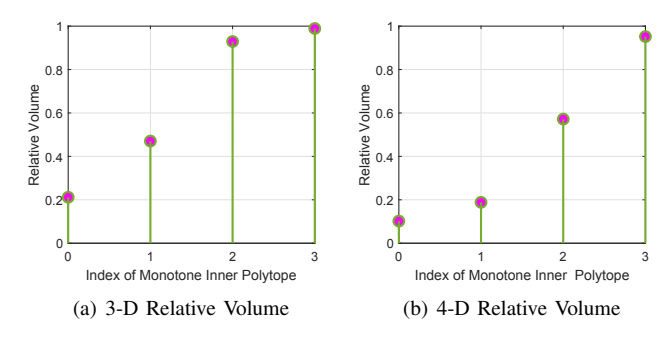


Fig. 7: Relative Volume of Inner Polytopes

Check Inner Polytope Approximation Check Feasibility Let 104 Let 105 Let 107 A-D Dimensionality of Loadability Region

Fig. 8: Execution Time of Screening Feasible Load Profiles

ACKNOWLEDGEMENT

We would like to acknowledge the helpful discussions with Prof. Paul Hines and Prof. Eytan Modiano, the support from NSF Award No. 1735513 and No. 1638331, and the support from the Khalifa University Award No. 8474000148.

REFERENCES

 R. Z. Ríos-Mercado and C. Borraz-Sánchez, "Optimization problems in natural gas transportation systems: A state-of-the-art review," *Applied Energy*, vol. 147, pp. 536–555, 2015.

- [2] M. Shahidehpour, Y. Fu, and T. Wiedman, "Impact of natural gas infrastructure on electric power systems," *Proceedings of the IEEE*, vol. 93, no. 5, pp. 1042–1056, 2005.
- [3] U.S. Energy Information Administration, "Short-term energy outlook." [Online]. Available, https://www.eia.gov/outlooks/steo/report/natgas.php.
- [4] S. An, Q. Li, and T. Gedra, "Natural gas and electricity optimal power flow," in *Transmission and Distribution Conference and Exposition*, 2003 IEEE PES, vol. 1, pp. 138–143, IEEE, 2003.
- [5] C. Liu, M. Shahidehpour, Y. Fu, and Z. Li, "Security-constrained unit commitment with natural gas transmission constraints," *IEEE Trans. Power Syst*, vol. 24, no. 3, pp. 1523–1536, 2009.
- [6] X. Zhang, M. Shahidehpour, A. S. Alabdulwahab, and A. Abusorrah,

- "Security-constrained co-optimization planning of electricity and natural gas transportation infrastructures," *IEEE Transactions on Power Systems*, vol. 30, no. 6, pp. 2984–2993, 2015.
- [7] M. Gil, P. Dueñas, and J. Reneses, "Electricity and natural gas interdependency: comparison of two methodologies for coupling large market models within the european regulatory framework," *IEEE Transactions on Power Systems*, vol. 31, no. 1, pp. 361–369, 2016.
- [8] M. Chertkov, S. Backhaus, and V. Lebedev, "Cascading of fluctuations in interdependent energy infrastructures: Gas-grid coupling," *Applied energy*, vol. 160, pp. 541–551, 2015.
- [9] A. Zlotnik, M. Chertkov, and K. Turitsyn, "Assessing risk of gas shortage in coupled gas-electricity infrastructures," in *System Sciences (HICSS)*, 2016 49th Hawaii International Conference on, pp. 2519–2527, IEEE, 2016
- [10] A. Zlotnik, L. Roald, S. Backhaus, M. Chertkov, and G. Andersson, "Coordinated scheduling for interdependent electric power and natural gas infrastructures," *IEEE Transactions on Power Systems*, vol. 32, no. 1, pp. 600–610, 2017.
- [11] K. A. Pambour, B. Cakir Erdener, R. Bolado-Lavin, and G. P. Dijkema, "Development of a simulation framework for analyzing security of supply in integrated gas and electric power systems," *Applied Sciences*, vol. 7, no. 1, p. 47, 2017.
- [12] H. Chen and R. Baldick, "Optimizing short-term natural gas supply portfolio for electric utility companies," *IEEE Transactions on Power Systems*, vol. 22, no. 1, pp. 232–239, 2007.
- [13] N. Judson, "Interdependence of the electricity generation system and the natural gas system and implications for energy security," tech. rep., MIT Lexington Lincoln Lab, 2013.
- [14] J. Mouawad, "Natural gas prices set record, pointing to costly winter," The New York Times, 2005.
- [15] G. Cimellaro, O. Villa, A. R. M. Bruneau, and H. Kim, "Resilience-based design of natural gas pipelines," in 15th World Conference in Earthquake Engineering, September, 2012.
- [16] G. P. Cimellaro, O. Villa, and M. Bruneau, "Resilience-based design of natural gas distribution networks," *Journal of Infrastructure systems*, vol. 21, no. 1, p. 05014005, 2014.
- [17] R. Carvalho, L. Buzna, F. Bono, M. Masera, D. K. Arrowsmith, and D. Helbing, "Resilience of natural gas networks during conflicts, crises and disruptions," *PloS one*, vol. 9, no. 3, p. e90265, 2014.
- [18] K. Poljanšek, F. Bono, and E. Gutiérrez, "Seismic risk assessment of interdependent critical infrastructure systems: the case of european gas and electricity networks," *Earthquake Engineering & Structural Dynamics*, vol. 41, no. 1, pp. 61–79, 2012.
- [19] K. Dvijotham, M. Vuffray, S. Misra, and M. Chertkov, "Natural gas flow solutions with guarantees: A monotone operator theory approach," arXiv preprint arXiv:1506.06075, 2015.
- [20] H. D. Nguyen, K. Dvijotham, and K. Turitsyn, "Constructing convex inner approximations of steady-state security regions," *IEEE Transactions* on *Power Systems*, vol. 34, no. 1, pp. 257–267, 2019.
- [21] G. K. Kamenev, "A class of adaptive algorithms for approximating convex bodies by polyhedra," *Zhurnal Vychislitel'noi Matematiki i Matematicheskoi Fiziki*, vol. 32, no. 1, pp. 136–152, 1992.
- [22] E. M. Bronstein, "Approximation of convex sets by polytopes," *Journal of Mathematical Sciences*, vol. 153, no. 6, pp. 727–762, 2008.
- [23] L. Marks, C. F. Mason, K. Mohlin, and M. Zaragoza-Watkins, "Vertical market power in interconnected natural gas and electricity markets," CESifo Working Paper Series, no. 6687, 2017.
- [24] P. M. Gruber, "Volume approximation of convex bodies by inscribed polytopes," *Mathematische Annalen*, vol. 281, no. 2, pp. 229–245, 1988.
- [25] P. M. Gruber, "Asymptotic estimates for best and stepwise approximation of convex bodies ii," in *Forum Mathematicum*, vol. 5, pp. 521–538, Walter de Gruyter, Berlin/New York, 1993.
- [26] G. K. Kamenev, "Analysis of an algorithm for approximating convex bodies," Zhurnal Vychislitel'noi Matematiki i Matematicheskoi Fiziki, vol. 34, no. 4, pp. 608–616, 1994.
- [27] K. Böröczky Jr, "Approximation of general smooth convex bodies," Advances in Mathematics, vol. 153, no. 2, pp. 325–341, 2000.
- [28] M. Naszódi, F. Nazarov, and D. Ryabogin, "Fine approximation of convex bodies by polytopes," arXiv preprint arXiv:1705.01867, 2017.
- [29] D. De Wolf and Y. Smeers, "The gas transmission problem solved by an extension of the simplex algorithm," *Management Science*, vol. 46, no. 11, pp. 1454–1465, 2000.

APPENDIX A PROOF OF CONVEXITY

Proof of Theorem 1: Let $\phi_a \in \mathcal{L}$ be a feasible load profile with the associated P_a , ψ_a and $K_{i,j,a}$. Let $\phi_b \in \mathcal{L}$ be another feasible load profile with the associated P_b , ψ_b and $K_{i,j,b}$. Consider

$$\phi_c := (1 - \mu)\phi_a + \mu\phi_b \tag{25}$$

where $\mu \in [0, 1]$. By Lemma 1 we know that $\psi_c = (1 - \mu)\psi_a + \mu \psi_b$ is the only branch flow profile.

Now let's remove the compressor and split the network \mathcal{G}_c into two sub-networks \mathcal{G}_1 and \mathcal{G}_2 .

Since

$$\phi_{i,c} = \psi_{i,j,c} = (1 - \mu)\psi_{i,j,a} + \mu\psi_{i,j,b}$$
 (26a)

$$\phi_{j,c} = \psi_{i,j,c} = (1 - \mu)\psi_{i,j,a} + \mu\psi_{i,j,b}$$
 (26b)

we have $\phi_{i,c} = \phi_{j,c}$ automatically. Therefore, for the split subnetworks, (10a) is the only constraint we need to consider at ϕ_c .

Consider \mathcal{G}_1 and \mathcal{G}_2 separately, Lemma 2 guarantees that each sub-network at least has one pressure profile. So we need to check if these pressure profiles are feasible and can be matched by (10a) for some $K_{i,j,c} \in [1,K_{max}]$. Mathematically, we need to show the following is non-empty.

$$P_{1,c} \geq P_{1,min} \tag{27a}$$

$$-P_{1,c} \geq -P_{1,max} \tag{27b}$$

$$\mathbf{C}_1 P_{1,c} = U_1 \tag{27c}$$

$$P_{2,c} \geq P_{2,min} \tag{27d}$$

$$-P_{2,c} \geq -P_{2,max} \tag{27e}$$

$$\mathbf{C}_2 P_{2,c} = U_2 \tag{27f}$$

$$K_{i,j,c}P_{1,i,c} - P_{2,j,c} = 0$$
 (27g)

$$K_{i,i,c} \geq 1$$
 (27h)

$$-K_{i,j,c} \geq -K_{max}$$
 (27i)

where $U_1 := ((1-\mu)\sqrt{\mathbf{C}_1P_{1,a}} + \mu\sqrt{\mathbf{C}_1P_{1,b}})^2$, $U_2 := ((1-\mu)\sqrt{\mathbf{C}_2P_{2,a}} + \mu\sqrt{\mathbf{C}_2P_{2,b}})^2$, subscript 1 and 2 indicate quantities associated with sub-network 1 and sub-network 2 respectively; subscript a and b represent quantities associated with the first feasible solution and the second feasible solution respectively.

Note that (27g)-(27i) is equivalent to the following

$$Ke_i P_{1,c} - e_j P_{2,c} \ge 0$$
 (28a)

$$-e_i P_{1,c} + e_j P_{2,c} \ge 0 \tag{28b}$$

where $K := K_{max}$ for simplicity, e_i and e_j are the row vectors that associate the fictitious nodes corresponds to the same compressor. Therefore, we need to show that the following primal problem (\mathcal{P}) is feasible.

$$min J_P = 0^T P_{1,c} + 0^T P_{2,c} (29a)$$

s.t.
$$P_{1,c} \ge P_{1,min}$$
 (29b)

$$-P_{1,c} \ge -P_{1,max} \tag{29c}$$

$$\mathbf{C}_1 P_{1,c} = U_1 \tag{29d}$$

$$P_{2,c} \ge P_{2,min} \tag{29e}$$

$$-P_{2,c} \ge -P_{2,max}$$
 (29f)

$$\mathbf{C}_2 P_{2,c} = U_2 \tag{29g}$$

$$Ke_i P_{1,c} - e_i P_{2,c} \ge 0$$
 (29h)

$$-e_i P_{1,c} + e_j P_{2,c} \ge 0 (29i)$$

Consider the dual problem (\mathcal{D})

s.t.
$$\alpha_1 - \beta_1 + \mathbf{C}_1^T \gamma_1 + K e_i^T \theta_1 - e_i^T \theta_2 = 0$$
 (30b)

$$\alpha_2 - \beta_2 + \mathbf{C}_2^T \gamma_2 - e_j^T \theta_1 + e_j^T \theta_2 = 0$$
 (30c)

$$\alpha_1, \beta_1, \theta_1, \alpha_2, \beta_2, \theta_2 \ge 0 \tag{30d}$$

$$\gamma_1, \gamma_2 \ free$$
 (30e)

Multiplying (30b) and (30c) on the left hand side with e_i and e_i , respectively

$$e_i(\alpha_1 - \beta_1 + \mathbf{C}_1^T \gamma_1) + K\theta_1 - \theta_2 = 0$$
 (31a)

$$e_j(\alpha_2 - \beta_2 + \mathbf{C}_2^T \gamma_2) - \theta_1 + \theta_2 = 0$$
 (31b)

Thus, we solve θ_1 and θ_2

$$\theta_1 = \frac{1}{1 - K} (e_i V_1 + e_j V_2)$$
 (32a)

$$\theta_2 = \frac{1}{1 - K} (e_i V_1 + K e_j V_2)$$
 (32b)

where $V_1 := \alpha_1 - \beta_1 + \mathbf{C}_1^T \gamma_1$ and $V_2 := \alpha_2 - \beta_2 + \mathbf{C}_2^T \gamma_2$. Substituting (32) into (30b) and (30c), and considering $\theta_1, \theta_2 \ge 0$ in (30d) we have

$$(I_1 - e_i^T e_i)V_1 = 0 (33a)$$

$$(I_2 - e_j^T e_j)V_2 = 0$$
 (33b)

$$e_i V_1 + e_i V_2 \leq 0 \tag{33c}$$

$$e_i V_1 + K e_i V_2 \leq 0 \tag{33d}$$

where I_1 and I_2 are the identity matrices associated with the two sub-networks.

Further define $\eta_1 := \alpha_1 - \beta_1$ and $\eta_2 := \alpha_2 - \beta_2$, then (33) is equivalent to

$$\eta_{1,k_1} = -C_{1,k_1}^T \gamma_1, \ k_1 \neq i$$
 (34a)

$$\eta_{2,k_2} = -C_{2,k_2}^T \gamma_2, \ k_2 \neq j$$
(34b)

$$\eta_{1,i} + \eta_{2,j} \le -C_{1,i}^T \gamma_1 - C_{2,i}^T \gamma_2$$
 (34c)

$$\eta_{1,i} + K\eta_{2,j} \le -C_{1,i}^T \gamma_1 - KC_{2,j}^T \gamma_2$$
 (34d)

where $\eta_{l,s}$ is the s-th entry of η_l , and $C_{l,s}^T$ is the s-th row of C_l^T , for l=1,2.

Considering the sum of positively scaled (34c) and (34d) we have

$$\zeta_1(\eta_{1,i} + \eta_{2,j}) + \zeta_2(\eta_{1,i} + K\eta_{2,j}) \le \zeta_1(-C_{1,i}^T\gamma_1 - C_{2,j}^T\gamma_2) + \zeta_2(-C_{1,i}^T\gamma_1 - KC_{2,j}^T\gamma_2)$$
(35)

where $\zeta_1, \zeta_2 \geq 0$.

Define $\omega_1 := \zeta_1 + \zeta_2$ and $\omega_2 := \zeta_1 + K\zeta_2$, then (35) is equivalent to

$$\omega_1 \eta_{1,i} + \omega_2 \eta_{2,j} \le -\omega_1 C_{1,i}^T \gamma_1 - \omega_2 \zeta_2 C_{2,j}^T \gamma_2 \tag{36}$$

for any ω_1 and ω_2 satisfying

$$\omega_2 - \omega_1 \geq 0 \tag{37a}$$

$$K\omega_1 - \omega_2 \ge 0 \tag{37b}$$

Inequality (36) will be revisited later in the proof.

Now let's replace α_1, α_2 by η_1, η_2 in the dual problem (\mathcal{D}) , and formulate an equivalent problem (\mathcal{D}_2)

$$max J_{D_2} = (P_{1,min}^T - P_{1,max}^T)\beta_1 + P_{1,min}^T \eta_1$$

$$+ (P_{2,min}^T - P_{2,max}^T)\beta_2 + P_{2,min}^T \eta_2$$

$$+ U_1^T \gamma_1 + U_2^T \gamma_2 (38a)$$

$$s.t.$$
 (34)

$$\beta_1 \ge -\eta_1 \tag{38c}$$

$$\beta_2 \ge -\eta_2 \tag{38d}$$

$$\beta_1, \beta_2 \ge 0 \tag{38e}$$

$$\gamma_1, \gamma_2, \eta_1, \eta_2 \ free$$
 (38f)

Since β_1, β_2 only appear in (38a), (38c), (38d), and (38e), we can further eliminate β_1, β_2 from problem (\mathcal{D}_2) and formulate a new equivalent problem (\mathcal{D}_3) .

$$max \quad J_{D_3} = (P_{1,min}^T - P_{1,max}^T) max[0, -\eta_1] + P_{1,min}^T \eta_1$$

$$+ (P_{2,min}^T - P_{2,max}^T) max[0, -\eta_2] + P_{2,min}^T \eta_2$$

$$+ U_1^T \gamma_1 + U_2^T \gamma_2$$
(39a)

$$s.t.$$
 (34)

$$\gamma_1, \gamma_2, \eta_1, \eta_2 \ free$$
 (39c)

where the $max[\cdot,\cdot]$ operator in (39a) takes pointwise maximum value.

Substituting (34a) and (34b) into (39a) yields

$$max \quad J_{D_{3}} = U_{1}^{T} \gamma_{1} + U_{2}^{T} \gamma_{2} + \left(\sum_{k_{1} \neq i} (P_{1,min,k_{1}} - P_{1,max,k_{1}}) max[0, C_{1,k_{1}}^{T} \gamma_{1}] \right. \\ + (P_{1,min,i} - P_{1,max,i}) max[0, -\eta_{1,i}] - \left. \sum_{k_{1} \neq i} P_{1,min,k_{1}} C_{1,k_{1}}^{T} \gamma_{1} + P_{1,min,i} \eta_{1,i} \right) + \left(\sum_{k_{2} \neq j} (P_{2,min,k_{2}} - P_{2,max,k_{2}}) max[0, C_{2,k_{2}}^{T} \gamma_{2}] \right. \\ + (P_{2,min,j} - P_{2,max,j}) max[0, -\eta_{2,j}] - \left. \sum_{k_{2} \neq j} P_{2,min,k_{2}} C_{2,k_{2}}^{T} \gamma_{2} + P_{2,min,j} \eta_{2,j} \right)$$
(40a)
$$s.t. \quad (34c), (34d) \quad (40b)$$

Problem (40) is equivalent to

 $\gamma_1, \gamma_2, \eta_1, \eta_2$ free

$$max \quad J_{D_3} = U_1^T \gamma_1 + U_2^T \gamma_2 + \left(-\sum_{k_1 \neq i} \tilde{P}_{1,k_1} C_{1,k_1}^T \gamma_1 + \tilde{P}_{1,i} \eta_{1,i} \right) + \left(-\sum_{k_1 \neq i} \tilde{P}_{2,k_2} C_{2,k_2}^T \gamma_2 + \tilde{P}_{2,j} \eta_{2,j} \right)$$
(41a)

(40c)

$$s.t.$$
 (34c), (34d) (41b)

 $\gamma_1, \gamma_2, \eta_1, \eta_2 \ free$ (41c)

where

$$\begin{split} \tilde{P}_{1,k_1} &= \begin{cases} P_{1,min,k_1}, & \text{if } C_{1,k_1}^T \gamma_1 < 0 \\ P_{1,max,k_1}, & \text{if } C_{1,k_1}^T \gamma_1 \geq 0 \end{cases} \\ \tilde{P}_{2,k_2} &= \begin{cases} P_{2,min,k_2}, & \text{if } C_{2,k_2}^T \gamma_2 < 0 \\ P_{2,max,k_2}, & \text{if } C_{2,k_2}^T \gamma_2 \geq 0 \end{cases} \\ \tilde{P}_{1,i} &= \begin{cases} P_{1,min,i}, & \text{if } \eta_{1,i} > 0 \\ P_{1,max,i}, & \text{if } \eta_{1,i} \leq 0 \end{cases} \\ \tilde{P}_{2,j} &= \begin{cases} P_{2,min,j}, & \text{if } \eta_{2,j} > 0 \\ P_{2,max,j}, & \text{if } \eta_{2,j} \leq 0 \end{cases} \end{split}$$

Note that (41a) can be bounded by

$$J_{D_{3}} \leq -\sum_{k_{1}\neq i} \hat{P}_{1,k_{1}} C_{1,k_{1}}^{T} \gamma_{1} + \hat{P}_{1,i} \eta_{1,i} + U_{1}^{T} \gamma_{1} + \sum_{k_{2}\neq i} \hat{P}_{2,k_{2}} C_{2,k_{2}}^{T} \gamma_{2} + \hat{P}_{2,j} \eta_{2,j} + U_{2}^{T} \gamma_{2}$$
(42)

as long as any $\hat{P}_{l,s} \in [P_{l,min,s}, P_{l,max,s}]$ for l=1,2 and every s. If $\hat{P}_{l,s}$ also satisfies (37), we have (36) which suggests that (42) is further bounded by B where

$$B = -\sum_{k_1 \neq i} \hat{P}_{1,k_1} C_{1,k_1}^T \gamma_1 - \hat{P}_{1,i} \gamma_1 + U_1^T \gamma_1$$
$$-\sum_{k_2 \neq j} \hat{P}_{2,k_2} C_{2,k_2}^T \gamma_2 - \hat{P}_{2,j} C_{2,j}^T \gamma_2 + U_2^T \gamma_2$$
$$= (U_1^T - \hat{P}_1^T C_1^T) \gamma_1 + (U_2^T - \hat{P}_2^T C_2^T) \gamma_2$$
(43)

According to Condition 3, we have $P_{l,max,s} = P_{max}$ and $P_{l,min,s} = P_{min}$ for all l=1,2 and s. So there exists at least a scalar P_0 in the intersection of all the pressure ranges. Substituting $\hat{P}_{l,s} = P_0$ in (43) for all l and s yields a specific bound denoted by B_0

$$B_{0} = B(\mathbf{1}P_{0}, \mathbf{1}P_{0}, \gamma_{1}, \gamma_{2})$$

$$= U_{1}^{T}\gamma_{1} + U_{2}^{T}\gamma_{2} - P_{0}(\mathbf{1}^{T}C_{1}^{T}\gamma_{1} + \mathbf{1}^{T}C_{2}^{T}\gamma_{2})$$

$$= U_{1}^{T}\gamma_{1} + U_{2}^{T}\gamma_{2}$$
(44)

On the other hand, consider $P_{1,\mu}=(1-\mu)P_{1,a}+\mu P_{1,b}$ and $P_{2,\mu}=(1-\mu)P_{2,a}+\mu P_{2,b}$. Since $(P_{1,a},P_{2,a})$ and $(P_{1,b},P_{2,b})$ are two feasible pressure profiles, they both satisfy (37). So $P_{1,\mu}$ and $P_{2,\mu}$ satisfy (37) as well. Thus, substituting $\hat{P}_1=P_{1,\mu}$ and $\hat{P}_2=P_{2,\mu}$ into (43) we have

$$J_{D_3} \leq B(P_{1,\mu}, P_{2,\mu}, \gamma_1, \gamma_2)$$

$$= (U_1^T - P_{1,\mu}^T C_1^T) \gamma_1 + (U_2^T - P_{2,\mu}^T C_2^T) \gamma_2$$

$$= -\mu (1 - \mu) (W_1^T \gamma_1 + W_2^T \gamma_2)$$
(45)

where
$$W_1 := \left(\sqrt{\mathbf{C}_1 P_{1,a}} - \sqrt{\mathbf{C}_1 P_{1,b}}\right)^2$$
 and $W_2 := \left(\sqrt{\mathbf{C}_2 P_{2,a}} - \sqrt{\mathbf{C}_2 P_{2,b}}\right)^2$.

Next, we are going to show that for any $B_0(\gamma_1^\star, \gamma_2^\star) > 0$ at some γ_1^\star and γ_2^\star , there exists another bound which is non-positive. The basic idea is to find a feasible pressure profile (P_1^\star, P_2^\star) satisfying (37) and making $B(P_1^\star, P_2^\star, \gamma_1^\star, \gamma_2^\star) \leq 0$.

Suppose at some given γ_1^{\star} and γ_2^{\star} we have $B_0 > 0$, consider the index set Ω associated with γ_1^{\star} and γ_2^{\star} such that

$$\Omega := \{ s \mid \gamma_{l,s}^{\star} > 0, \ l = 1, 2 \} \tag{46}$$

We are going to construct the desired pressure profile $(P_1^{\star}, P_2^{\star})$ in the following way. To start with, let the set of source node be S, and assign each source node pressure to P_{max} temporarily.

- 1) Pick an unvisited source node $i_s \in S$, record its downstream node pressures until reaching the first merging node, say, i_m . The downstream pressures are assigned successively by the following way: if a branch from node-n to node m with pressure P_n determined and P_m undetermined. If the corresponding $\gamma \notin \Omega$, taking $P_m = P_n$; else, taking $P_m = P_n P_{\mu,n} + P_{\mu,m}$, where $P_{\mu,m} = (1-\mu)P_{a,m} + \mu P_{b,m}$ and $P_{\mu,n} = (1-\mu)P_{a,n} + \mu P_{b,n}$.
- 2) Consider a merging node- i_m with m many branches entering it. For every entering branch denote its upstream node index set (including i_m) as I_k , where $k=1,\cdots,m$. If all the node pressures for every set I_k have been assigned, the pressure P_{im} on node- i_m has m choices $\{P_{im,1},\cdots,P_{im,m}\}$. Take P_{im} as the minimum value $P_{im,min}$ from $\{P_{im,1},\cdots,P_{im,m}\}$. Update the node pressures P_{I_k} for every set I_k by $P_{I_k}-P_{im,k}+P_{im,min}$.
- 3) If a merging node- i_m and all of its upstream node pressures have been determined, adding i_m as a new source node to S. Repeat Step 1) and 2) until every node pressure is determined.

This process eventually provides us a desired pressure profile $(P_1^{\star}, P_2^{\star})$. Firstly, it is a feasible pressure profile in the sense of being within pressure limits. Since the source pressures have been assigned to P_{max} at the beginning, in Step 1 a downstream pressure $P_n \ge P_{\mu,n}$ by the monotonicity of pressure along the flow direction. In Step 2, since every $P_{im,k} \geq P_{\mu,im}$, we also have $P_{im} \geq P_{\mu,im}$ at current step (but can be updated by a further Step 2). However, the last merging node which has no downstream merging node will retain the pressure $P_{im} \geq P_{\mu,im}$ because no further Step 2 will be executed. It serves as the only source node for the rest undetermined nodes as well. Therefore, by repeating Step 1, any downstream pressure $P_n \geq P_{\mu,n}$. By Condition 3 from Section IV, since $P_{min} \leq P_{\mu} \leq P_{max}$, we also have $P_{min} \leq$ $P^{\star} \leq P_{max}$. On the other hand, we assign the compressor's output pressure P_{output} as the value of $min(KP_{input}^{\star}, P_{max})$, where P_{input}^{\star} is the determined compressor's input pressure. Then $P_{output} \ge P_{\mu,output}$ as well. Hence, the same arguments also hold for the compressor's downstream subgraph.

Let's substitute $(P_1^\star, P_2^\star, \gamma_1^\star, \gamma_2^\star)$ in B. It actually replaces each positive term associated with $\gamma^\star \in \Omega$ by the corresponding non-positive term in $B(P_{1,\mu}, P_{2,\mu}, \gamma_1^\star, \gamma_2^\star)$. Thus, $B(P_1^\star, P_2^\star, \gamma_1^\star, \gamma_2^\star) \leq 0$. Therefore, we have shown that $J_{D_3} \leq 0$ for every (γ_1, γ_2) , suggesting that the dual problem is bounded. By the *strong duality theorem of linear programming*, the primal problem (\mathcal{P}) is feasible, which concludes the convexity.

APPENDIX B PARAMETERS OF MODIFIED BELGIUM GAS NETWORK

TABLE I: Node Parameters

Node Index	Type	Load (kSCM/min)	π_{max} (Bar)	π_{min} (Bar)
1	2	0	66	30
2	2	0	66	30
3	1	2.7208	66	30
4	1	0	66	30
5	2	0	66	30
6	1	2.8014	66	30
7	1	1.6500	66	30
8	2	0	66	30
9	1	0	66	30
10	1	6.4200	66	30
11	1	0	66	30
12	1	3.4720	66	30
13	1	8.0000	66	30
14	1	9.0000	66	30
15	1	2.7560	66	30
16	1	1.8400	66	30
17	1	0	66	30
18	1	0	66	30
19	1	1.1540	66	30
20	1	2.0000	66	30
21	3	0	66	30
22	3	0	66	30
23	3	0	66	30
24	3	0	66	30

Type 1 is the load node. Type 2 is the source node. Type 3 is the fictitious node associated with a compressor.

kSCM/min means 10³ standard cubic meters per minute

TABLE II: Source Parameters

Node Index	ϕ_{max} (kSCM/min)	ϕ_{min} (kSCM/min)
1	18.1	0
2	6.4	0
5	23.8	0
8	21.5	0

TABLE III: Pipeline and Compressor Parameters

From Node	To Node	λ
1	2	17.496668
2	3	11.664448
3	4	2.672950
5	6	8.048349
6	7	4.071689
7	4	4.109421
4	11	8.318121
8	21	8.810786
22	9	8.810786
9	10	2.101347
10	11	2.881077
11	12	1.416588
12	13	1.437417
13	14	3.499335
14	15	1.749667
15	16	0.699865
11	17	0.024809
17	23	0.046192
24	18	2.006192
18	19	1.000821
19	20	0.013416
From Node	To Node	K_{max}
21	22	1.5
23	24	1.5



Dan Wu received the B.S. degree in electrical engineering and automation from the Huazhong University of Science and Technology, Wuhan, China, in 2012. He received the M.S. and Ph.D. degrees from the University of Wisconsin Madison, Madison, WI, USA, in 2014 and 2017, respectively. He was a Postdoctoral Associate at the Mechanical Engineering Department, Massachusetts Institute of Technology (MIT) from 2017 to 2018, and now is a Postdoctoral Associate at the Laboratory for Information and Decision Systems, MIT. His research includes

nonlinear dynamics and optimization, electric power system analysis, natural gas networks, interdependent complex systems, algebraic and topological methods in engineering applications.



and management.

Tiantian Nie was an Assistant Professor in Department of Systems Engineering and Engineering Management at University of North Carolina at Charlotte during 2017 - 2018. She was awarded a BS in Mathematics in 2012 from Tsinghua University. She received an MS in 2013 and a PhD in 2016, in Industrial Systems and Engineering from North Carolina State University at Raleigh. Her research interests are in theory of nonlinear and discrete optimization, and optimization-based approaches for analytical decision making in operations research



Konstantin Turitsyn received his M.Sc. degree in physics from the Moscow Institute of Physics and Technology, Dolgoprudny, Russia, and his Ph.D. degree in physics from the Landau Institute for Theoretical Physics, Moscow, Russia, in 2007. He was an Associate Professor with the Mechanical Engineering Department, Massachusetts Institute of Technology (MIT), Cambridge, MA, USA until 2018. Before joining MIT, he held the position of Oppenheimer Fellow with Los Alamos National Laboratory, and Kadanoff Rice Postdoctoral Scholar

with the University of Chicago. His research interests encompass a broad range of problems involving nonlinear and stochastic dynamics of complex systems. Specific interests in energy related fields include stability and security assessment, integration of distributed and renewable generation.



Seth Blumsack is Professor of Energy Policy and Economics and International Affairs in the John and Willie Leone Family Department of Energy and Mineral Engineering at Pennsylvania State University. He is also on the External Faculty of the Santa Fe Institute. His research interests include coupled engineered, social and natural systems; reliability and resilience in electric power systems; reliability and resilience in electric power systems; electricity market design; and the governance of Regional Transmission Organizations. He earned his B.A. in Math and Economics from Reed College, his M.S.

in Economics from Carnegie-Mellon University, and his Ph.D. in Engineering and Public Policy from Carnegie-Mellon University.